

The Formation History of Subhalos and the Evolution of Satellite Galaxies

JINGJING SHI,^{1,2} HUIYUAN WANG,^{3,4} HOUJUN MO,^{5,6} MARK VOGELSBERGER,⁷ LUIS C. HO,^{1,8} MIN DU,¹ DYLAN NELSON,⁹
ANNALISA PILLEPICH,¹⁰ AND LARS HERNQUIST¹¹

¹*Kavli Institute for Astronomy and Astrophysics, Peking University, Beijing 100871, China*

²*Kavli IPMU (WPI), UTIAS, The University of Tokyo, Kashiwa, Chiba 277-8583, Japan*

³*Key Laboratory for Research in Galaxies and Cosmology, Department of Astronomy, University of Science and Technology of China, Hefei, Anhui 230026, China*

⁴*School of Astronomy and Space Science, University of Science and Technology of China, Hefei 230026, China*

⁵*Department of Astronomy, University of Massachusetts, Amherst MA 01003-9305, USA*

⁶*Astronomy Department and Center for Astrophysics, Tsinghua University, Beijing 10084, China*

⁷*Kavli Institute for Astrophysics and Space Research, Massachusetts Institute of Technology, Cambridge, MA 02139, USA*

⁸*Department of Astronomy, School of Physics, Peking University, Beijing 100871, China*

⁹*Max-Planck-Institut für Astrophysik, Karl-Schwarzschild-Str. 1, 85741 Garching, Germany*

¹⁰*Max-Planck-Institut für Astronomie, Königstuhl 17, 69117 Heidelberg, Germany*

¹¹*Harvard-Smithsonian Center for Astrophysics, 60 Garden Street, Cambridge, MA 02138*

ABSTRACT

Satellites constitute an important fraction of the overall galaxy population and are believed to form in dark matter subhalos. Here we use the cosmological hydrodynamic simulation TNG100 to investigate how the formation histories of subhalos affect the properties and evolution of their host galaxies. We use a scaled formation time (a_{nf}) to characterize the mass assembly histories of the subhalos before they are accreted by massive host halos. We find that satellite galaxies in young subhalos (low a_{nf}) are less massive and more gas rich, and have stronger star formation and a higher fraction of ex situ stellar mass than satellites in old subhalos (high a_{nf}). Furthermore, these low a_{nf} satellites require longer timescales to be quenched as a population than the high a_{nf} counterparts. We find very different merger histories between satellites in fast accretion (FA, $a_{\text{nf}} < 1.3$) and slow accretion (SA, $a_{\text{nf}} > 1.3$) subhalos. For FA satellites, the galaxy merger frequency dramatically increases just after accretion, which enhances the star formation at accretion. While, for SA satellites, the mergers occur smoothly and continuously across the accretion time. Moreover, mergers with FA satellites happen mainly after accretion, while a contrary trend is found for SA satellites. Our results provide insight into the evolution and star formation quenching of the satellite population.

Keywords: Galaxy evolution (594), Cosmology (343), Hydrodynamical simulations (767)

1. INTRODUCTION

In the prevailing paradigm of galaxy formation, galaxies grow in dark matter halos, built via gravitational collapse of small density peaks in the early Universe. Within halos, baryonic gas cools radiatively and condenses. The gas is then converted into stars, forming galaxies (Rees & Ostriker 1977; White & Rees 1978; Fall & Efstathiou 1980). Halos grow hierarchically by accreting smaller structures. These small structures become substructures (subhalos) of host halos, and

galaxies within them become satellite galaxies, orbiting around the central galaxies residing in the deep gravitational potential wells of the host halos. Many studies use various methods to determine the satellite abundance and suggest that about 30% of galaxies with stellar mass $\sim 10^9 M_{\odot}/h$ are satellites, while the satellite fractions decrease with increasing stellar mass (Mandelbaum et al. 2006; Tinker et al. 2007; van den Bosch et al. 2008; Yang, Mo & van den Bosch 2008; Wetzel et al. 2013; Bray et al. 2016). Satellite galaxies apparently constitute a non-negligible population of the entire galaxy population.

After being accreted, satellites are believed to experience some specific processes that can quench ongo-

ing star-formation or even cause morphological transformation. For example, subhalos and satellite galaxies stop growing, or lose their mass due to the strong tidal stripping of host halos (e.g. Gunn & Gott 1972); some satellites even get tidally disrupted (e.g. into intra-cluster light) before merging with the centrals (Mihos et al. 2005; Wetzel & White 2010; Bahé et al. 2019); dynamical friction gradually reduces the orbital angular momentum so that the satellites sink towards the halo center (Chandrasekhar 1943a,b,c); ram pressure can remove the hot halo gas reservoir or even the cold gas in the disk of satellites (Gunn & Gott 1972; Ayromlou et al. 2019; Yun et al. 2019); ‘harassment’ from neighbouring galaxies can tidally heat the satellite system (Farouki & Shapiro 1981); satellite-satellite mergers can affect both the star formation activity and morphology (Makino & Hut 1997; Wetzel, Cohn & White 2009). However, the importance of these processes in quenching/transforming satellites, and their dependence on various halo properties is still under debate.

In observations, satellites have been studied in great detail. Based on the group catalog built by Yang et al. (2005), Weinmann et al. (2006) found that the fraction of early-type/late-type satellites varies with halo mass, and further showed that early-type satellites have a tendency to surround early-type centrals (called ‘galactic conformity’, see also Kauffmann et al. 2013; Tinker et al. 2018; Calderon, Berlind & Sinha 2018). van den Bosch et al. (2008) investigated the efficiency of satellite specific processes by comparing the color and concentration of satellites and centrals of the same stellar mass at $z = 0$ (see also Peng et al. 2010, 2012; Wang et al. 2018c). These studies assume that centrals at $z = 0$ closely resemble the progenitors of satellites at the time when they are being accreted by host halos. However, such assumptions ignore the evolution of galaxies (see for example Pannella et al. 2009; Newman et al. 2012; Stark et al. 2013; Barro et al. 2017; Genzel et al. 2017; Tadaki et al. 2017; Price et al. 2019). Subsequently, Yang et al. (2012) and Wetzel et al. (2013) took evolution into account and used an empirical parameterization method to derive the initial star formation rate (SFR) of satellites at the accretion time, and further investigated the quenching time scale of satellites. In their methods, it is assumed that at the time of accretion, satellite progenitors resemble central galaxies of the same stellar mass. This assumption, however, still needs to be verified.

These satellite specific processes can be investigated in theoretical galaxy formation models, such as semi-analytical models (SAMs), hydrodynamical simulations, and halo-based models. In SAMs, these processes are included in a parameterized way. The efficiencies and scal-

ings that characterize these processes are constrained by fitting simultaneously the observed stellar mass functions and quenched fractions at various redshifts (see Henriques et al. 2015 for example). These models reasonably reproduce the observed red fractions of galaxies as a function of stellar mass in varying environments across several redshifts, the satellite passive fractions as a function of halo mass, and the projected distance from the central galaxies, and the clustering signal for blue and red galaxies (Henriques et al. 2017). However, significant differences between model predictions and observations are also presented in the literature (Hirschmann et al. 2014; Wang et al. 2018a,b). These studies suggest that the SAMs require an improvement in the environmental processes in order to reduce the differences between centrals and satellites. In fact, the detailed treatment of the environmental processes varies from model to model. For example, the earlier versions usually assume an instantaneous stripping of hot gas around satellites once they fall into their hosts (see Croton et al. 2006; Bower et al. 2006), while subsequent models allow for a gradual loss of the hot gas (Font et al. 2008; Kang & van den Bosch 2008; Weinmann et al. 2010; Guo et al. 2011; Hirschmann et al. 2014).

Halo-based models have often been used to study the connection between galaxies and dark matter halos (e.g. Jing, Mo & Börner 1998; Berlind & Weinberg 2002; Yang, Mo & van den Bosch 2003). In the subhalo abundance matching methods (SHAMs, see Kravtsov et al. 2004; Vale & Ostriker 2004; Conroy, Wechsler & Kravtsov 2006), galaxies are populated within subhalos and a tight correlation between galaxy stellar mass and halo properties, such as halo mass, is adopted. In particular, satellite galaxies are assumed to follow the same stellar mass - halo mass (SMHM) relation as centrals. However, the halo mass-based SHAMs fail to reproduce small scale clustering measurements, which are usually dominated by satellites (Yang et al. 2012; Behroozi, Wechsler & Conroy 2013; Moster, Naab & White 2013; Rodríguez-Puebla et al. 2017). Campbell et al. (2018) suggested that the discrepancy could be caused by some simple assumptions that are not valid in reality. For example, the models neglect the contribution of ‘orphan’ galaxies, the mass growth of satellites after their accretion, and the influence of halo assembly history. In fact, persistent star formation after accretion is found to be important for understanding the bimodality of satellites (Weinmann et al. 2009; Kang & van den Bosch 2008; Wang et al. 2007; Simha et al. 2009; Wetzel, Cohn & White 2009). In addition, tidal stripping of stars (Mihos et al. 2005) and satellite-satellite mergers (Wetzel,

Cohn & White 2009) may be also important since they alter the SMHM relations.

All satellite-specific processes, such as tidal stripping, ram pressure, and galaxy interactions, are environmental effects that can be simulated by solving the equations for collisionless dynamics and hydrodynamics (see Vogelsberger et al. 2019 for a review on cosmological simulations). In particular, hydrodynamical simulations can account for these satellite-specific processes in a self-consistent manner, although the results should be interpreted with caution because of limited numerical resolutions and uncertainties in subgrid models. The predicted satellite stellar mass function at a given halo mass from simulations matches local observations (Bahé et al. 2017). Wright et al. (2019) studied the quenching timescales of galaxies in EAGLE simulations for centrals and satellites, finding that different physical mechanisms are at play for galaxies of low, intermediate, and high mass. Bahé & McCarthy (2015) showed that ram pressure stripping is the main mechanism that is responsible for satellite quenching in groups and clusters using GIMIC cosmological hydrodynamical simulations. Yun et al. (2019) and Jung et al. (2018) studied the efficiency of ram pressure in removing the gas content of satellites using TNG100 and HorizonAGN. Joshi et al. (in preparation) demonstrates with the TNG50 and TNG100 simulations that group and cluster environments transform galaxies from disc to spheroids, possibly because of tidal shocking. Using different suites of hydrodynamical simulations, others have shown how the disruption rate, tidal mass loss, specific star formation rate, luminosity-weighted age, stellar metallicity, and alpha element abundance ratios of satellites depend on the time since infall (Rhee et al. 2017; Pasquali et al. 2019; Bahé et al. 2019). Engler et al. (in preparation) show that satellite and central galaxies lie on distinct average relations between stellar mass and current dynamical mass in TNG100. However, most previous works focus on how satellites evolve after accretion, without considering in detail the role of the formation history of the subhalos prior to accretion.

More recently, Shi et al. (2018) studied the formation history of subhalos before they are accreted by more massive host halos. Interestingly, they find that there are two infall subhalo populations, which correspond to the fast-accretion and slow-accretion phases found in normal distinct halos (Zhao et al. 2003). They also compared these infall subhalos with normal halos at the time of accretion and found that infall subhalos are usually younger than normal halos of the same halo mass. The different halo growth histories of those two infall subhalo populations may leave an imprint on the satellites

at $z = 0$. In addition, the difference between infall subhalos and normal halos raises the question of whether the satellite progenitors before accretion are different from general centrals at the time of accretion. In this work, we use the cosmological hydrodynamical simulations IllustrisTNG to carry out investigations on satellite galaxies and infall subhalos, focusing on how the formation history of infall subhalos influence the initial status of satellites and their further evolution.

The structure of the paper is organized as follows. In section 2, we briefly introduce the IllustrisTNG simulations, our sample selection, and definitions adopted in this work. In section 3, we present our results, focusing on the role of the formation history on satellites/the difference between satellites and centrals at the time of accretion, evolution after accretion, and the state at $z=0$. In section 4 we discuss the implications of our work for SHAMs and satellite quenching. We summarize our main results in section 5.

2. METHOD

2.1. The ILLUSTRIS-TNG Simulations

Throughout this work, we use the data from the IllustrisTNG simulations (Naiman et al. 2018; Marinacci et al. 2018; Springel et al. 2018; Pillepich et al. 2018b; Nelson et al. 2018, 2019a; Pillepich et al. 2019) that feature a novel model for AGN feedback, magneto-hydrodynamics, a new scheme for galactic winds, and updated choices for stellar evolution and chemical enrichment (for more details on the TNG model, see Weinberger et al. 2018; Pillepich et al. 2018b; Nelson et al. 2019b), leading to significant improvements over the original Illustris model (Vogelsberger et al. 2013, 2014b,a; Genel et al. 2014). To study the evolution of satellite galaxies, we use the highest resolution run of the $\sim 100\text{Mpc}$ box TNG100-1 (TNG100 hereafter), which is performed with the moving-mesh code AREPO (Springel 2010; Weinberger, Springel & Pakmor 2019) in a periodic box of $75\text{Mpc}/h$ on a side. It follows the dynamical evolution of 1820^3 DM particles and approximately 1820^3 gas cells or stellar/wind particles from $z = 127$ to $z = 0$, producing 100 snapshots between $z = 20$ and $z = 0$. The cosmological parameters of the IllustrisTNG simulations are consistent with recent Planck measurements (Planck Collaboration et al. 2016): $\Omega_m = 0.3089$, $\Omega_b = 0.0486$, $\Omega_\Lambda = 0.6911$, $\sigma_8 = 0.8159$, $n_s = 0.9667$ and $h = 0.6774$.

Halos and structures within them, for example galaxies, are identified by using the Friends-of-Friends (FOF) and SUBFIND algorithms (Davis et al. 1985; Springel et al. 2001). Usually, each FOF group contains one or more SUBFIND structures (hereafter substructure or

subhalo) and the baryonic component in a substructure is defined as a galaxy. In this paper, FOF halos are referred to as halos or host halos. The most massive substructure in a FOF halo is classified as a central subhalo and its galaxy is regarded as the central galaxy of the halo. The other substructures (if they exist) are called satellite subhalos, the baryonic components of which are referred to as satellite galaxies. We verified that our results do not change when we select satellites that are within the virial radius of host halos. To be concise, we use the term “satellites (or centrals)” to refer to both satellite (or central) galaxies and satellite (or central) subhalos in the following text.

The subhalos (including both central and satellite subhalos) are connected across the 100 snapshot outputs by the SUBLINK algorithm (Rodriguez-Gomez et al. 2015). The descendant of a subhalo is identified by matching the weighted baryons in the next snapshot (i.e. lower redshift), where the most bound particles/cells have the highest priorities. Each subhalo has only one descendant, yet it can have more than one progenitor. The main progenitor is defined as the one with the ‘most massive history’ behind it (De Lucia & Blaizot 2007). In this way, merger trees are constructed.

We also use the data from the original Illustris simulation and TNG300-1 to verify the dependencies of our results on the parameterized sub-grid physics and the numerical resolution. Most of our results remain the same across the three sets of simulations.

2.2. Sample and galaxy properties

We first describe the definitions of some common parameters used in this paper for halos and galaxies.

- *Halo mass*: the mass contained in the spherical region (centered on the most bounded particle) where the mean mass density is equal to $200\rho_{\text{crit}}(z)$. Note that halo mass is only measured for central subhalos.
- *Galaxy stellar mass*: the sum of all stellar particles within twice the stellar half mass radius, $2R_*$, where R_* is defined using all stellar particles within the subhalo.
- *Galaxy gas mass*: the sum of all the mass in gas cells within $2R_*$.
- *Specific star formation rate ($s\text{SFR}$)*: star formation rate (SFR) per unit stellar mass, where SFR is computed by summing up the star formation rates in all star-forming gas cells within $2R_*$.
- *Ex situ stellar mass fraction $f_{\text{ex situ}}$* : the fraction of stellar mass that is formed in other galaxies and accreted later by the galaxy (Rodriguez-Gomez et al. 2017). This parameter can be used to quantify the contribution of galaxy mergers to the mass growth.

We select all satellite galaxies at $z = 0$ and trace them back in time along their merger trees. Below, we list some parameters and phrases, which can record the evolution history of satellite galaxies and subhalos, and describe them briefly:

- *Accretion time z_{peak}* : the redshift when the subhalo of a satellite galaxy is a central subhalo and its halo mass reaches the maximum during its lifetime. Therefore, z_{peak} is usually thought to be the time when the subhalo starts to be influenced by the gravitational field of its host halo.
- *Peak halo mass M_{peak}* : the halo mass at z_{peak} .
- *Satellite and Central phases*: The central phase is the time when a $z = 0$ satellite galaxy is a central galaxy (i.e. at $z > z_{\text{peak}}$), and the satellite phase is the time after being accreted by a more massive host halo (i.e. at $z < z_{\text{peak}}$).
- *Formation time z_f and a_{nf}* : z_f is the redshift when the subhalo of a satellite galaxy is a central subhalo and its subhalo reaches half of its peak mass, $M_{\text{peak}}/2$, for the first time. Also, $a_{\text{nf}} \equiv (1 + z_f)/(1 + z_{\text{peak}})$ is the formation redshift scaled by the accretion redshift. z_f and a_{nf} therefore reflect the formation history of a subhalo during its central phase.
- *FA, SA1 and SA2 populations*: Subhalos with $a_{\text{nf}} < 1.3$ are classified as the fast accretion (FA) population; those with $a_{\text{nf}} > 1.3$ are classified as the slow accretion (SA) population (Shi et al. 2018). As we do not know whether they grow because of accretion (e.g. of “smooth” DM) or assembly (i.e. of merging with other DM haloes), we could stick to one name but then it could mean both physical processes. The SA population is further divided into SA1 ($1.3 < a_{\text{nf}} < 1.8$) and SA2 ($a_{\text{nf}} > 1.8$) samples. See Section 3.1 for more details.

The quantities with subscript ‘0’ denote the values measured at $z = 0$ and those with subscript ‘peak’ denote the values at z_{peak} . For example, M_0 and M_{peak} denote the halo mass at $z = 0$ and z_{peak} respectively, while $M_{*,0}$ and $M_{*,\text{peak}}$ mean the stellar mass at $z = 0$ and z_{peak} respectively. In this paper, we mainly focus on satellite galaxies residing in host halos

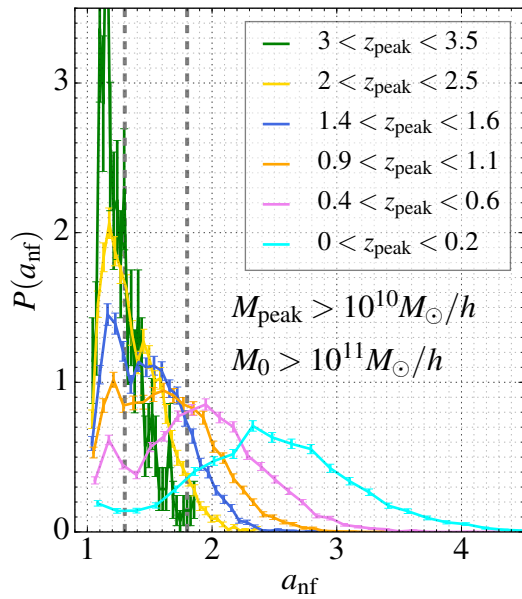


Figure 1. Distribution of the scaled formation time, $a_{\text{nf}} \equiv (1 + z_f)/(1 + z_{\text{peak}})$, for TNG100 satellite subhalos that survived at $z = 0$ and are accreted at different redshifts, where z_f is the formation time and z_{peak} is the accretion time, as defined in section 2.2. Here we include only the satellites with $M_{\text{peak}} > 10^{10} M_{\odot}/h$ and host halo mass $M_0 > 10^{11} M_{\odot}/h$. The gray dashed vertical lines indicate the division thresholds for the FA, SA1, and SA2 populations. The error bars are Poisson errors.

of $M_0 > 10^{11} M_{\odot}/h$ at $z = 0$ and having peak halo mass $M_{\text{peak}} > 10^{10} M_{\odot}/h$. For comparison, we also relate the satellite galaxies to the central galaxies. We note that a galaxy that is identified as a satellite at $z = 0$ was actually a central galaxy in its central phase. *To avoid any confusion, we always call it a satellite galaxy, even in its central phase.*

3. RESULTS

The main purpose of this paper is to investigate whether and how, for a satellite at $z = 0$, its formation history in its central phase affects or leaves an imprint on its evolution in its satellite phase and final state, and to understand the different evolutionary paths between centrals and satellites. In Section 3.1, we first show the formation time distribution for these satellites and the separation of fast and slow accretion populations. In Section 3.2, we present results on the stellar mass - halo mass (SMHM) relation. The evolution of stellar mass, gas content, and star formation are presented in Section 3.3 and Section 3.4. We also present the satellite quenched fraction in 3.5. Finally, in Section 3.6, we

present results about galaxy mergers for these satellite galaxies.

3.1. Bimodal formation time distribution of infall subhalos

In our previous work (Shi et al. 2018), we found that the scaled formation time (a_{nf}) distribution of the satellite subhalos is bimodal at a given accretion time z_{peak} , using a cosmological N-body simulation. The result is confirmed here with the cosmological hydrodynamical simulation TNG100, as shown in Figure 1. Our tests in Shi et al. (2018) with much larger N-body simulations suggest that such bimodality is independent of the host halo mass at $z = 0$ and depends only weakly on peak halo mass M_{peak} .

In Shi et al. (2018), we demonstrated that the bimodality in normalized formation time a_{nf} is closely connected to the two accretion phases (fast and slow accretion phases) found in the mass accretion history of dark matter halos (Zhao et al. 2003). The peak with small a_{nf} corresponds to the subhalos that are in the fast-accretion phase (i.e. younger), while the population with large a_{nf} corresponds to the subhalos that are in the slow-accretion phase (i.e. older). It should be noted that the infall time distribution of satellite galaxies selected to be found within the virial radius from a more massive host is bimodal as well, even when infall is defined as virial radius crossing. In that case, the bimodality is removed when backsplash satellites are included, i.e. those are outside the virial radius at given time (Yun et al. 2019; Engler et al., in preparation). Since the a_{nf} distribution of FA halos is narrow and its peak is always around 1.2, almost independent of z_{peak} , host halo mass, and M_{peak} (Shi et al. 2018), we adopt the demarcation value $a_{\text{nf}} = 1.3$ to divide them into FA and SA populations (see Figure 1). The fractions of the two populations are a strong function of z_{peak} . Satellite subhalos that are accreted at $z_{\text{peak}} > 2.3$ (roughly 11 Gyr ago) are mainly FA halos, while those accreted later are dominated by SA halos.

As we will show below, satellites in the FA and SA satellite galaxies evolve in different ways, in particular in the satellite phase. There are two possible origins for the difference. One is that FA and SA satellites are distinct populations, as suggested by the bimodal a_{nf} distribution. The other is that the difference simply reflects a continuous change as a function of a_{nf} , since they, by definition, have different formation times. To distinguish the two possibilities, in principle, one should divide the sample into many small a_{nf} bins, then check how the satellite properties and their evolution vary with a_{nf} . However, due to the limited number of satel-

lites (as shown in Table 1), we adopt a coarse binning method, in which the FA population is kept unchanged and the SA population is split into two subsamples, SA1 ($1.3 < a_{\text{nf}} < 1.8$) and SA2 ($a_{\text{nf}} > 1.8$). We choose this approach because the FA population has a much narrower a_{nf} distribution than the SA population. The demarcation value of 1.8 is chosen so that the three populations have roughly a comparable number of galaxies (see the other vertical dashed line in figure 1). Table 1 briefly lists the number of satellites in each subsample. If a satellite property changes smoothly across the three samples, i.e. FA, SA1, and SA2, the property is very likely determined by halo formation history. If a special feature for a property appears in FA, but is totally absent in SA1 and SA2, it implies that FA and SA are indeed different in this property.

Table 1. Number of satellites in each subsample of varying z_{peak} bins that correspond to different lines in Figure 1.

z_{peak}	FA	SA1	SA2
0 – 0.2	186	367	3154
0.4 – 0.6	754	1624	3091
0.9 – 1.1	1181	2277	1627
1.4 – 1.6	1518	2285	720
2 – 2.5	2021	2097	228
3 – 3.5	329	165	5

3.2. Stellar mass - halo mass relation

The stellar mass-halo mass (SMHM) relation can provide valuable constraints on the efficiency in transforming gas into stars and has been studied in great detail in the literature (e.g. Yang, Mo & van den Bosch 2003; Zheng, Coil & Zehavi 2007; Yang, Mo & van den Bosch 2008, 2009; Behroozi, Conroy & Wechsler 2010; Guo et al. 2010; Wang & Jing 2010; Yang et al. 2012; Wechsler & Tinker 2018; Pillepich et al. 2018a). In this subsection, we present the SMHM relations for the three samples of satellites and central galaxies. In order to understand the evolution of the relations, two kinds of SMHM relations are investigated as shown in Figure 2. The first one is the $z = 0$ SMHM relation, in which halo mass (M_{halo}) is taken as the halo mass at z_{peak} (M_{peak}) for satellites and halo mass at $z = 0$ (M_0) for centrals. The second one is the z_{peak} SMHM relation. In this relation, for both centrals and satellites, stellar mass and halo mass at z_{peak} are adopted.

We first show the $z = 0$ SMHM relations for satellite and central galaxies in the upper-left panel of Figure 2. To check the dependence on accretion time, we select

three z_{peak} ranges ($0.4 < z_{\text{peak}} < 0.6$, $1.0 < z_{\text{peak}} < 1.5$ and $1.6 < z_{\text{peak}} < 2.6$), and show results in these z_{peak} ranges in the same panel. Since the simulation box is quite small, we only show the SMHM relation in a relatively narrow halo mass range (from about $10^{10.5}$ to $10^{12.5} M_{\odot}/h$). As one can see, for both centrals and satellites, $M_{\star,0}$ is strongly correlated with halo mass, with a scatter of about 0.25 dex. It is in good agreement with previous studies (Yang, Mo & van den Bosch 2009; More et al. 2011; Moster, Naab & White 2013; Behroozi, Wechsler & Conroy 2013; Zu & Mandelbaum 2015; Matthee et al. 2017). Moreover, the SMHM relations for satellites are consistent with that for centrals, and almost independent of the accretion time z_{peak} , as shown by the non-solid lines. We then show the z_{peak} SMHM relations at three z_{peak} ranges in the lower-left panel. Similar to the $z = 0$ relation, centrals and satellites almost follow the same relation. Furthermore, there is only weak evolution with redshift, which is consistent with the independence of the $z = 0$ SMHM relation on accretion time. All of these results suggest that host halo mass (or M_{peak}) is the major factor that governs the galaxy stellar mass over a wide range of redshift for both centrals and satellites. Note that all this applies when the halo mass of satellites are considered at z_{peak} , i.e. before any environmental effect. In fact, the $z = 0$ relations between current stellar and dynamical mass are clearly distinct for satellite and central galaxies (Engler et al., in preparation).

We then investigate the z_{peak} SMHM relation for the three satellite samples with different a_{nf} separately (the lower right panel of Figure 2). At a given halo mass, $M_{\star,\text{peak}}$ increases gradually from the lowest a_{nf} sample (FA, youngest) to the highest a_{nf} sample (SA2, oldest). This suggests that the z_{peak} SMHM relation changes continuously with a_{nf} . In addition, the a_{nf} dependence slightly decreases with increasing M_{peak} . Our further tests show that the z_{peak} SMHM relations for the three samples are all independent of z_{peak} , consistent with the results shown in the lower left panel of Figure 2. Recently, several works (Matthee et al. 2017; Zehavi et al. 2018; Artale et al. 2018) studied the output of SAMs and hydrodynamical simulations and found that, at fixed halo mass, old halos tend to host more massive central galaxies at $z = 0$. For instance, Artale et al. (2018) found that the oldest 20% halos host galaxies that are ~ 0.4 dex larger than the youngest 20% halos. This is broadly consistent with our findings.

At $z = 0$, the difference among the three satellite samples is apparently reduced, but still significant (upper right panel of Figure 2). The maximum difference of about 0.25 dex appears at $M_{\text{peak}} < 10^{11.5} M_{\odot}/h$

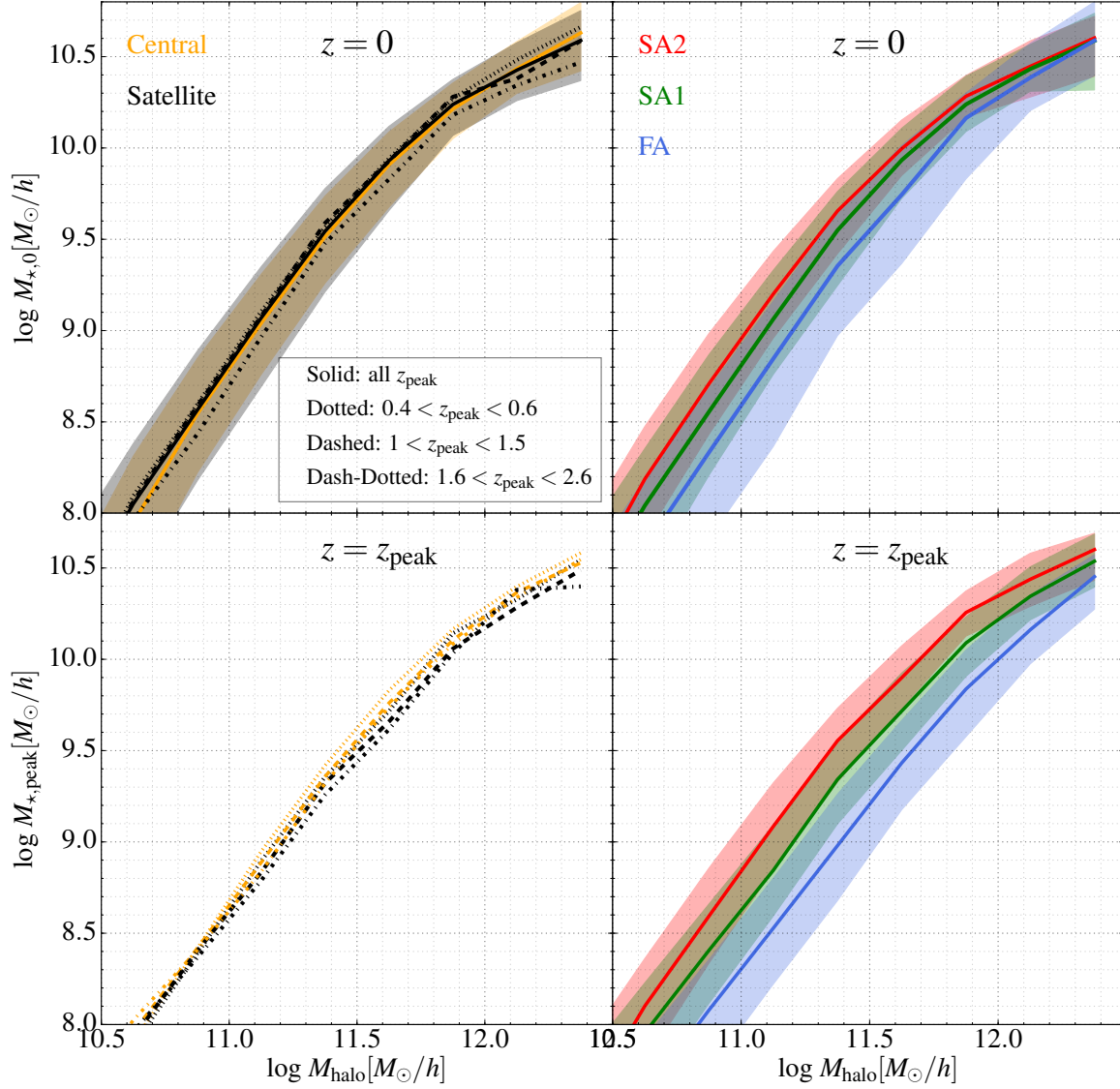


Figure 2. Stellar mass to halo mass relation from TNG100. Here M_{halo} is M_0 for centrals and M_{peak} for satellites. Upper left: the $z=0$ SMHM relation for the satellites (black lines) and centrals (orange lines). The dotted, dashed, and dash-dotted lines show the relation for satellites accreted at different z_{peak} bins, as indicated by the label. Lower left: The z_{peak} SMHM relation for satellites at three z_{peak} bins and centrals at the corresponding redshifts. See the text for more details. Upper right: the median $z=0$ SMHM relation for FA (blue), SA1 (green), and SA2 (red) satellites. The shaded area shows the 1σ dispersion around the median relations. Lower right: The SMHM relation at z_{peak} for satellites. Color and line types are the same as the upper right panel.

and the difference decreases with increasing M_{peak} . At $\log M_{\text{peak}} \sim 11.9$ ($\log M_{\star,0} \sim 10.2$), the difference becomes negligible. We also check the dependence of the $z = 0$ SMHM relation on accretion time and no significant dependence is found. By comparing the z_{peak} and $z = 0$ SMHM relations, we find that satellites grow with time in the satellite phase, but the growth amplitude decreases with increasing a_{nf} . We will discuss this in more detail in the following. These results suggest that there is a time delay between halo assembly and galaxy assembly. So even when a halo becomes a substructure of another massive halo and starts to lose its mass, the galaxies within it can still grow (see also Fig. 8 of Engler et al., in preparation).

3.3. Stellar mass assembly

To see more clearly how the stellar mass of satellites evolves with time, we select satellites with two $M_{\star,\text{peak}}$ ranges and three z_{peak} ranges and present their stellar mass evolution in Figure 3. For comparison, we also show the evolution of the corresponding central galaxies in the same figure. These central galaxies have stellar masses comparable to these satellites, and are classified as centrals at redshifts close to z_{peak} , regardless of whether or not they are classified as centrals at other redshifts. We first check the mass growth of these satellite galaxies in their central phase (i.e. $z > z_{\text{peak}}$). The mass growth for satellites as a whole (black solid lines) resembles that for centrals (orange solid lines). Moreover, satellites with high a_{nf} (older) grow at a longer timescale and more slowly than centrals, while satellites with low a_{nf} (younger) grow faster than the corresponding centrals.

At the beginning of the satellite phase, satellites continue to grow, although the growth rate appears to be slowed down. On average, the satellites stop growing at $\log[(1+z)/(1+z_{\text{peak}})] \sim -0.1$, which corresponds to a time scale from 1.3 Gyr (at $z = 2$) to 2.7 Gyr (at $z = 0.5$). The halo dynamical time scales at $z = 2$ and $z = 0.5$ are about 0.5 Gyr and 1.1 Gyr, so the mass growth ceases roughly at 2 times the dynamical time scale after accretion, likely due to the lack of gas supply (see Section 3.4). For satellites that are accreted at low redshift ($z_{\text{peak}} \sim 0.5$ and $z_{\text{peak}} \sim 1.2$), the stellar mass remains unchanged after reaching its peak; while the satellites accreted at high redshift (e.g. $z_{\text{peak}} \sim 2$) eventually lose mass by a factor of 0.2 dex after reaching a maximum. This is possibly due to tidal stripping, since these satellites are accreted earlier and tend to reside in the inner region of their host halos at $z = 0$, where the tidal field is the strongest (Gnedin, Hernquist & Ostriker 1999). After being accreted, satellites with

smaller a_{nf} (younger) apparently grow faster and more (about 0.4 dex) than satellites with larger a_{nf} (older), ranging from 0.15 to 0.25 dex. The growth rate decreases with increasing a_{nf} , consistent with the results shown in the SMHM relations (see the left panels of figure 2). This is saying that the stellar mass growth relies on a_{nf} in both central and satellite phases, and the difference between FA and SA populations does not relate to the bimodality of a_{nf} .

3.4. Gas content and star formation

Galaxies grow their mass mainly via two ways, star formation and mergers. In this subsection, we analyze the gas content and star formation of the satellites and how they evolve with time. In the left panels of Figure 4, we show the gas to stellar mass ratio and specific star formation rate (sSFR) at accretion time as a function of stellar mass. As before, three z_{peak} ranges are adopted. In this plot, the sSFRs of galaxies with a vanishing sSFR value (i.e. $\text{sSFR} < 10^{-14} \text{yr}^{-1}$) are set to be 10^{-14}yr^{-1} by hand; galaxies with vanishing gas content are also included when calculating the median values. We can see that galaxies with small stellar mass or at high redshift tend to be more gas rich. This is consistent with previous studies (e.g. Genzel et al. 2015; Tacconi et al. 2018; Caletto et al. 2018). The sSFR shows a similar correlation with redshift, but a different correlation with stellar mass. As one can see, sSFR is almost independent of stellar mass at $\log M_{\star,\text{peak}} < 10$ and then quickly drops as the stellar mass increases. The drop in sSFR at the massive end is caused by the kinetic-mode AGN feedback in the TNG model, which tends to quench star formation (Donnari et al. 2019; Terrazas et al. 2019; Weinberger et al. 2018). We also show the results for central galaxies at three snapshots with redshifts close to the considered z_{peak} in the right panels. Again, centrals are very similar to these satellites at all stellar mass and redshift bins in consideration.

We then check whether these properties vary with a_{nf} . The results are presented in the right panels of Figure 4. The satellites in subhalos with the lowest a_{nf} (youngsters, blue lines) have largest gas content and the highest sSFR at z_{peak} . However, as shown in Figure 1, a_{nf} is anti-correlated with z_{peak} . So the correlations with a_{nf} might be caused by the correlations with z_{peak} . To check this, we investigate the a_{nf} dependence in several narrow z_{peak} bins. We find that the gas content and sSFR increase as the a_{nf} decreases even when z_{peak} is fixed (these results are not plotted to avoid showing a very crowded figure). This is consistent with results shown in the SMHM relation and mass evolution that

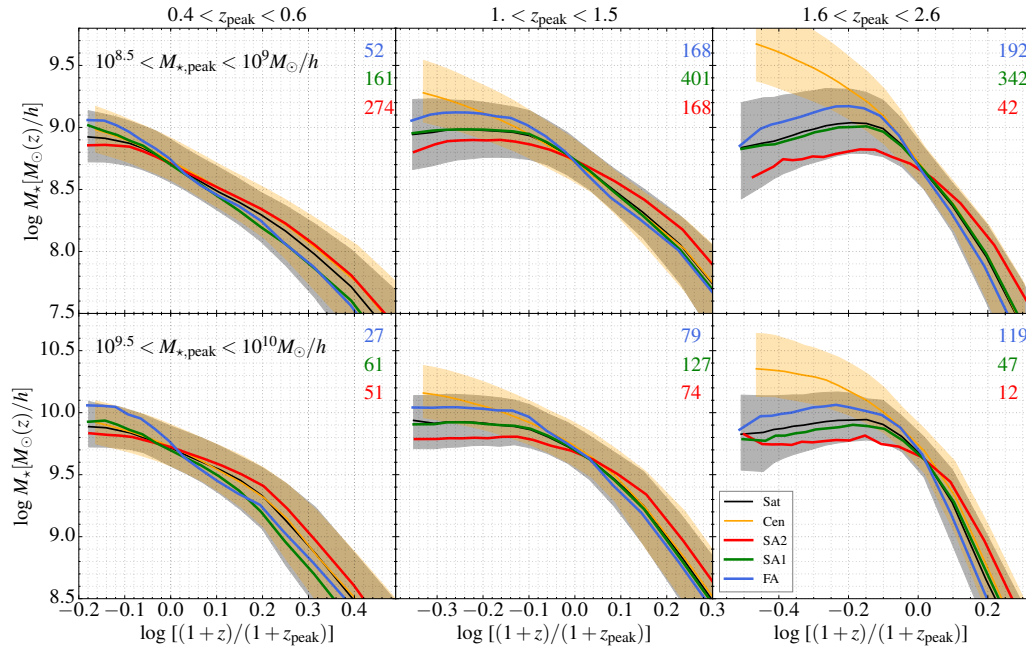


Figure 3. Stellar mass assembly of TNG100 galaxies. The solid lines show the median stellar mass evolution for different satellite samples as indicated in the panels and the corresponding centrals. These central galaxies have stellar masses similar to the satellites, and are classified as centrals at a redshift close to z_{peak} , regardless of whether or not they are classified as centrals at other redshifts. The shaded black and orange areas show the 1σ dispersion of the evolution for the satellites and centrals. The numbers in each panel show the number of satellites that we have for each subsample. The same statistics applies to Figure 5, 8, and 10.

the satellites with smaller a_{nf} (younger) grow faster than satellites with larger a_{nf} (older).

Figure 5 shows the evolution of sSFR with time. Since the evolution of gas to stellar mass ratio is similar to sSFR, we only show results for sSFR. Similar to Figure 3, the results for two $M_{*,\text{peak}}$ ranges and three z_{peak} ranges are presented as an example. The results for central galaxies are also presented as a benchmark. First of all, central galaxies exhibit a continuous and steady decline in star formation with redshifts, consistent with previous studies in both simulations and observations (van de Voort et al. 2011; Bahé & McCarthy 2015; Sales et al. 2015). This is likely due to the continuous decline of gas amount with decreasing redshift (see e.g. Figure 4). Second, in the central phase, satellites as a whole have almost the same evolutionary history as centrals. This explains why the stellar mass evolution is the same for centrals and satellites in the central phase (see Section 3.2). Third, in the satellite phase ($z < z_{\text{peak}}$), compared to centrals, the star formation activity in satellites declines much more quickly. This is apparently ascribed to satellite-specific processes, such as strangulation, ram pressure stripping and tidal stripping (Ostriker & Tremaine 1975; Peng, Maiolino & Cochrane

2015; Yun et al. 2019; Bahé & McCarthy 2015). Fourth, in both central and satellite phases, satellites of low a_{nf} (younger) have slightly stronger star formation activities than high a_{nf} (older) ones. Our tests show that, for a given accretion time, low a_{nf} satellites are, on average, more gas rich than high a_{nf} satellites throughout the entire central and satellite phases. It can thus be used to understand why the low a_{nf} satellites grow faster than high a_{nf} ones (see Figure 2 and 3). Fifth, we observe an apparent enhancement of star formation activity around z_{peak} for FA satellites. This enhancement is completely absent for the central galaxies and the SA satellite populations. We also see a similar enhancement in gas to stellar mass ratio. We will come back to this interesting phenomenon later.

3.5. Quenched fractions

Finally, we investigate the status of satellites at $z = 0$. Since a large fraction of satellites contain no gas particles and have no star formation activity at $z = 0$, we show quenched fractions instead of gas content and sSFR. The quenched fraction is the fraction of galaxies with sSFR less than 10^{-11}yr^{-1} (see e.g. Donnari et al. 2019 for the discussion of the quenched galaxy definition

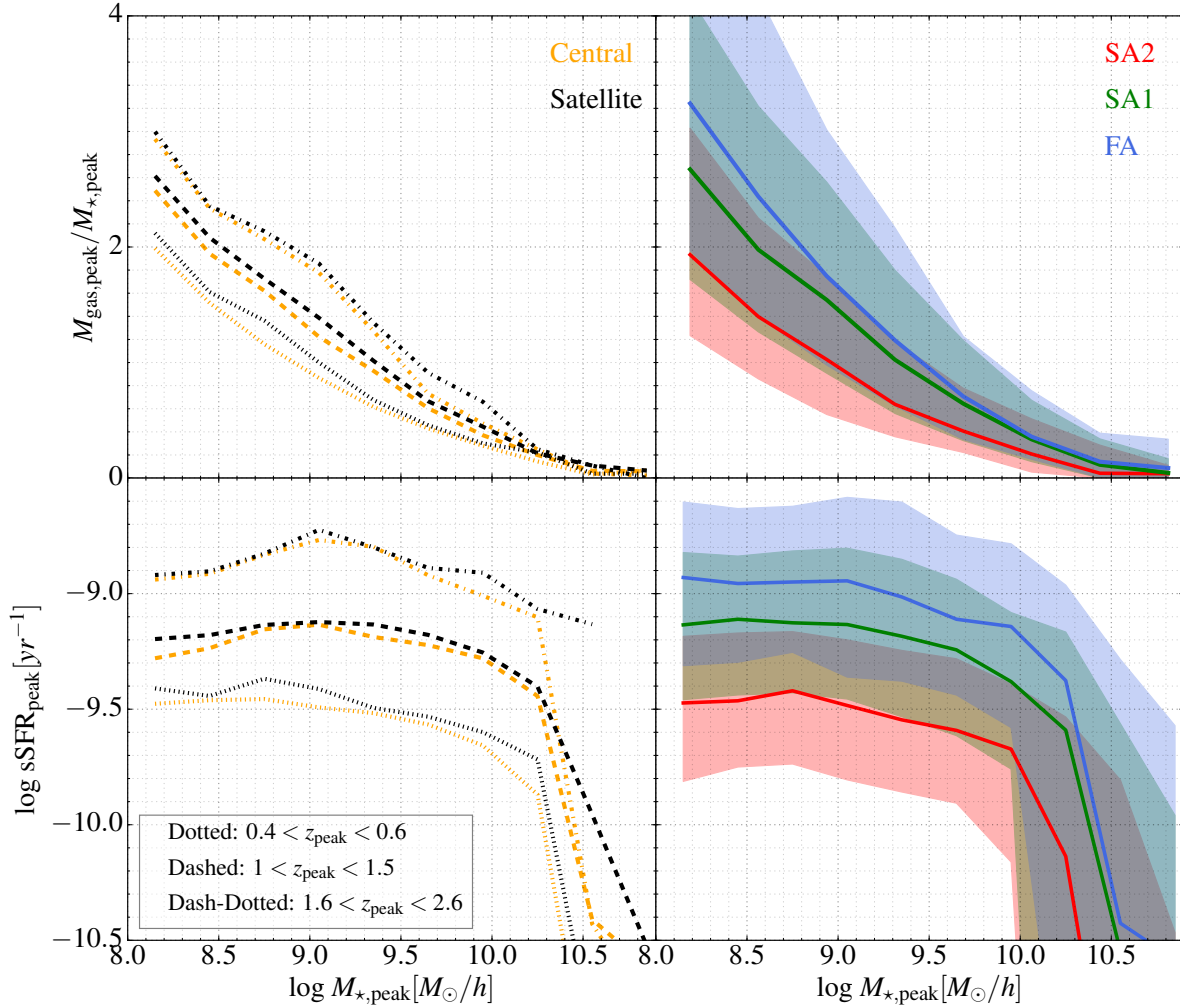


Figure 4. Median gas mass fractions and sSFRs in TNG100 galaxies. Left column: gas to stellar mass ratio (top) and sSFR (bottom) for centrals (orange) and satellites (black) in various z_{peak} bins. Right column: gas to stellar mass ratio (top) and sSFR (bottom) as a function of the stellar mass at z_{peak} for the three satellite populations. Note that in this plot, we set the sSFR of quenched galaxies ($\text{sSFR} < 10^{-14} \text{yr}^{-1}$) to be 10^{-14}yr^{-1} by hand.

in TNG100). Figure 6 shows the quenched fractions as a function of stellar mass. As expected, satellites are more frequently quenched than centrals of the same stellar mass, due to the satellite-specific processes. A detailed comparison of satellite quenched fractions with observational data will be useful (Donnari et al. 2020, in preparation).

We also show the quenched fractions for satellites with different halo assembly histories separately. Interestingly, as a whole, the quenched fractions for FA satellites (younger, blue solid lines) are higher than the SA satellites (older, green and red solid lines). This appears

to be in conflict with the results that low a_{nf} satellites usually contain more gas and have higher star formation activity (see Figure 4 and 5). To understand this discrepancy, we show the quenched fractions for satellites accreted at two z_{peak} ranges in the lower panel. As one can see, satellites accreted earlier are more frequently quenched than those accreted later. At a given z_{peak} , the quenched fraction increases with increasing a_{nf} , consistent with the results shown above. Since low a_{nf} satellites are usually accreted earlier than high a_{nf} satellites (see Figure 1), the dependence of the quenched

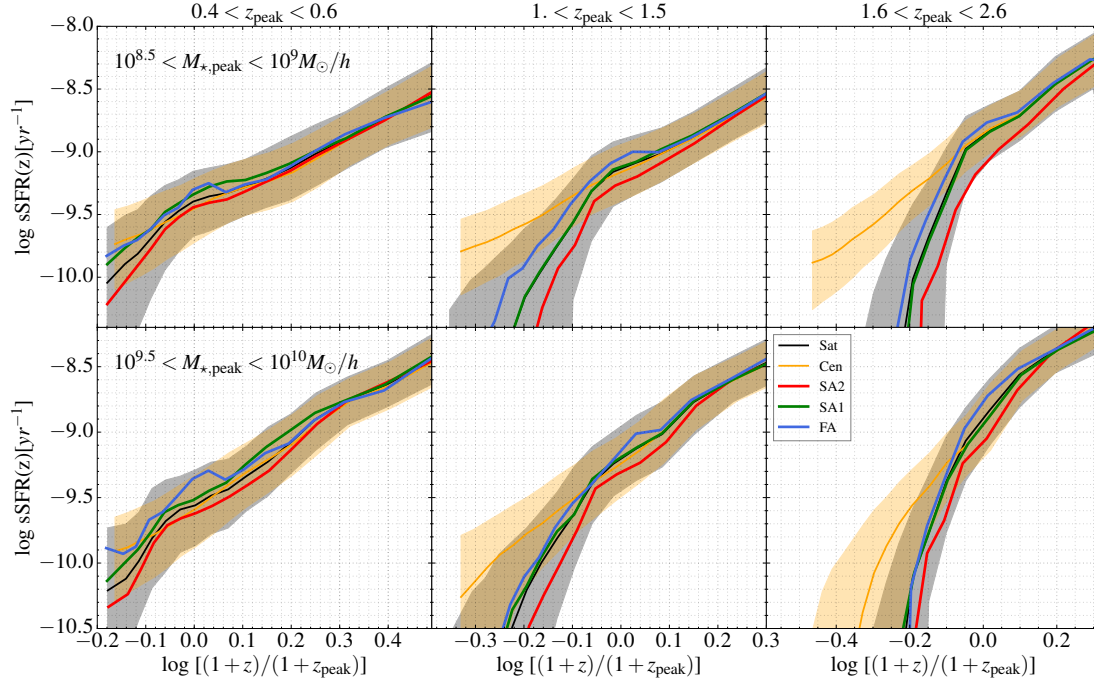


Figure 5. Similar to figure 3, but for the sSFR evolution of satellites and centrals from TNG100.

fraction on a_{nf} in the whole satellite sample (the upper panel in Figure 6) is therefore explained.

3.6. Galaxy stellar mass accretion and mergers

Galaxy mergers play an important role in mass growth and morphological transformation. It is thus interesting to investigate the importance and frequency of galaxy mergers for satellites. We first use $f_{\text{ex situ}}$ (see Section 2.2 for the definition) to quantify the importance of galaxy mergers. In Figure 7, we show $f_{\text{ex situ}}$ at accretion ($f_{\text{ex situ,peak}}$) and at $z = 0$ ($f_{\text{ex situ,0}}$) for satellites with different z_{peak} and a_{nf} . The results for the corresponding centrals are also presented for comparison. On average, $f_{\text{ex situ}}$ is low, ranging from 0.03 to 0.3, indicating that in situ star formation dominates the stellar mass growth for most galaxies with $M_{\star,0} < 10^{10} M_{\odot}/h$ (See Lu et al. (2015), see also Pillepich et al. 2018a for the ex situ stellar mass fractions at larger galaxy masses). One common feature among these centrals and satellites of different a_{nf} at different redshifts is that $f_{\text{ex situ}}$ is almost constant with stellar mass at $\log M_{\star} < 10.0$, and rapidly increases with stellar mass at the massive end. Such behavior is quite similar to sSFR and quenched fractions shown in Figure 4 and 6. One likely reason for the similarity is that, in TNG, galaxy mergers can cause the growth of supermassive black holes and trigger AGN feedback, which can cease star formation in host galax-

ies. This hints that galaxy mergers play an important (or even dominant) role in triggering AGN feedback and quenching star formation in TNG (see Tacchella et al. 2019 for an in depth discussion of this in the TNG100 simulation).

As we can see, there is no significant difference in $f_{\text{ex situ,peak}}$ between central and satellites. At $z = 0$, centrals and satellites also have quite similar $f_{\text{ex situ,0}}$ at a given stellar mass, on average. This means that environment has little effect on $f_{\text{ex situ}}$. However, the dependence of $f_{\text{ex situ}}$ on z_{peak} and a_{nf} appears to evolve with time. At z_{peak} time, $f_{\text{ex situ,peak}}$ is almost independent of z_{peak} , while at redshift zero, we observe a strong dependence. Moreover, at accretion time, satellites with small a_{nf} tend to have slightly larger $f_{\text{ex situ,peak}}$ than their counterparts with large a_{nf} . At $z = 0$, the difference becomes larger, in particular between FA and SA1. These results imply that some specific processes occur in the satellite phase, as we will see below.

To better understand the results shown above, we present the evolution of $f_{\text{ex situ}}$ for two $M_{\star,\text{peak}}$ bins and three z_{peak} bins in Figure 8. Central galaxies exhibit a mass dependent evolution. For the less massive galaxies, in general, $f_{\text{ex situ}}$ decreases with time, indicating that in situ star formation is more important at low redshift. For massive galaxies selected at low redshift, $f_{\text{ex situ}}$ almost does not evolve with time, while for

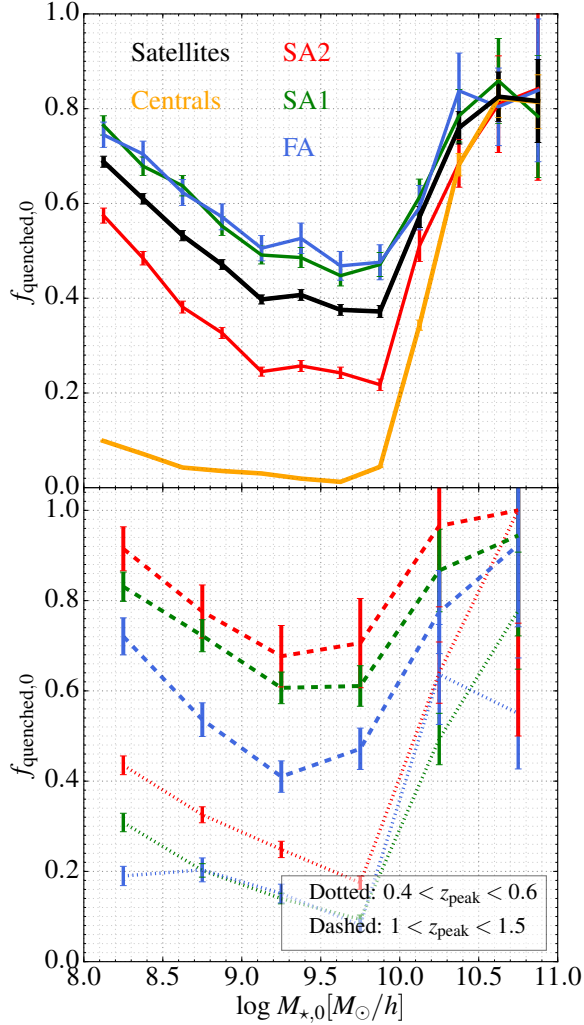


Figure 6. Quenched fractions at $z = 0$ in TNG100. Upper panel: quenched fractions at $z = 0$ as a function of the stellar mass for centrals, satellites as a whole and satellites of different a_{nf} . Lower panel: quenched fractions at $z = 0$ as a function of the stellar mass for the three satellite populations accreted at $1 < z_{\text{peak}} < 1.5$ (dashed) and $0.4 < z_{\text{peak}} < 0.6$ (dotted). Satellites in the $1.6 < z_{\text{peak}} < 2.6$ bin are almost all quenched at $z = 0$, but the results are not plotted for clarity. The error bars are Poisson errors.

massive galaxies selected at high redshift, $f_{\text{ex situ}}$ first decreases then increases as cosmic time passes. This is apparently the result of the competition between star formation and mergers. These results are broadly consistent with [Rodríguez-Gomez et al. \(2017\)](#). However, the detailed processes responsible for such evolution is

beyond the scope of this paper and we will mainly focus on the behavior of satellites.

In the central phase ($z > z_{\text{peak}}$), the difference among centrals, FA, SA1, and SA2 populations are generally small. The significant lower values of SA2 (red lines) in $1.6 < z_{\text{peak}} < 2.6$ bin is mainly caused by poor statistics. It is consistent with the results at z_{peak} shown in Figure 7. We note that, at $z_{\text{peak}} \sim 0.5$, the results for FA satellites are significantly different from others. This is very likely due to the fact that the FA population at low redshift is relatively small (see e.g. Figure 1). In the satellite phase, satellites deviate from the tracks of centrals and the deviation becomes larger and larger with time. For satellites accreted at low redshift ($z_{\text{peak}} < 1.5$), the difference between centrals and satellites at $z = 0$ is small, but for those accreted at $z_{\text{peak}} > 1.6$, the deviation is very large. In fact, we observe a persistent and strong decrease of $f_{\text{ex situ}}$ for satellites of high z_{peak} , very different from their central counterparts. In the satellite phase, the stellar mass growth is small and occurs only at the beginning (see Section 3.2 and Figure 3), so the persistent decrease of $f_{\text{ex situ}}$ cannot be primarily ascribed to the contribution of in situ star formation. One possible reason is that tidal stripping is more efficient for accreted stars since they are usually located in the outer regions of the galaxies.

In the satellite phase, FA (blue line) and SA (green and red lines) galaxies exhibit very different evolutionary tracks in $f_{\text{ex situ}}$. We observe a ‘burst’ of $f_{\text{ex situ}}$ around z_{peak} for FA satellites, particularly at low z_{peak} . This means that a large fraction of the FA population experiences merger events around z_{peak} . It is usually believed that mergers can enhance the star formation rate ([Mihos & Hernquist 1996](#)). Indeed, we also observe an enhancement in star formation activity, as shown in Figure 5). However, no signal for such merger events is found for the two SA samples. This explains why the difference in $f_{\text{ex situ}}$ between FA and SA populations becomes larger at $z = 0$ (Figure 7).

We can also quantify the importance of galaxy mergers by counting the number of merger events during the history of a galaxy. We define mergers with $M_{*,\text{prog}}/M_{*,0} > 0.2$ as major mergers and $0.05 < M_{*,\text{prog}}/M_{*,0} < 0.2$ as minor mergers, where $M_{*,0}$ is the stellar mass of a galaxy at $z = 0$ and $M_{*,\text{prog}}$ is the maximum stellar mass of its merging companion. We note that, the conventional definition for merger types uses the ratio of two stellar masses at the moment when mergers happen. However, one of our main concerns is whether galaxy mergers eventually affect the galaxy at $z = 0$, we thus classify major and minor merger by comparing

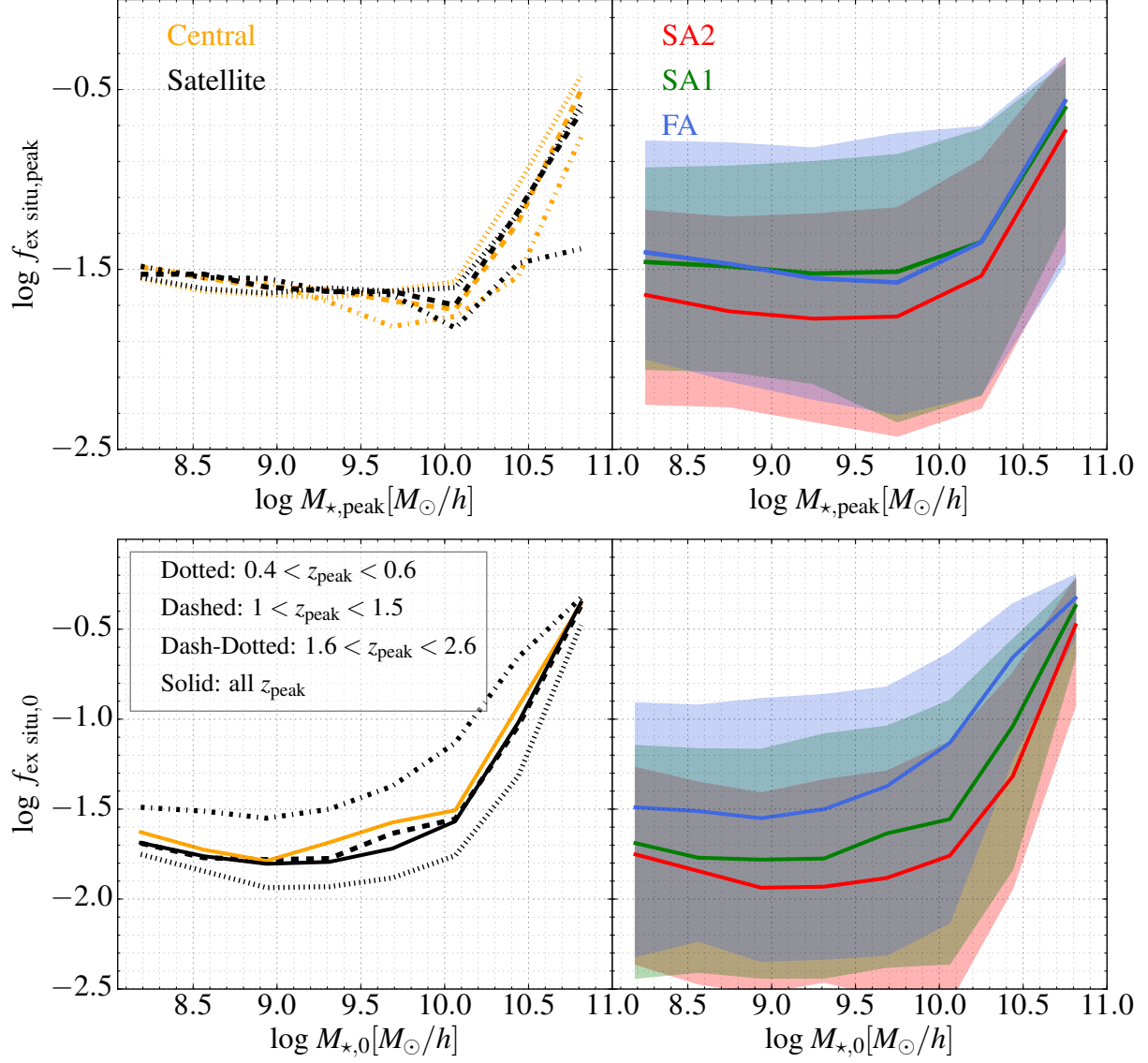


Figure 7. Ex situ stellar mass fractions for TNG100 galaxies. Upper left: the ex situ stellar mass fractions as a function of stellar mass for satellite galaxies at different z_{peak} and centrals at corresponding redshifts. Upper right: the ex situ stellar mass fractions as a function of the stellar mass for the three satellite populations at z_{peak} . Lower panels: the ex situ stellar mass fractions at $z = 0$. Solid lines show the results for all z_{peak} , while dashed-dotted, dotted, and dashed lines show the results for satellites with different z_{peak} . The black and orange lines show the relation for satellites and centrals at $z = 0$. The shaded areas are the 1σ dispersion around the relation.

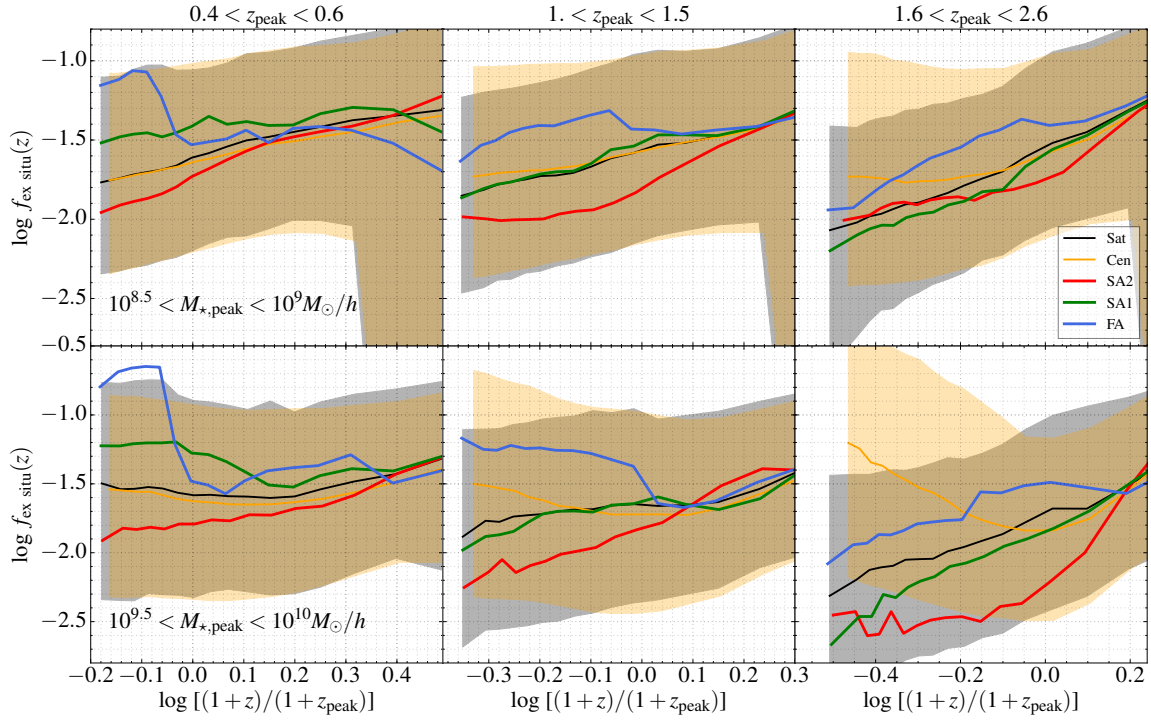


Figure 8. Similar to Figure 3, but for the evolution of the accreted stellar mass fractions (i.e. the ex situ stellar mass fractions) of galaxies in TNG100.

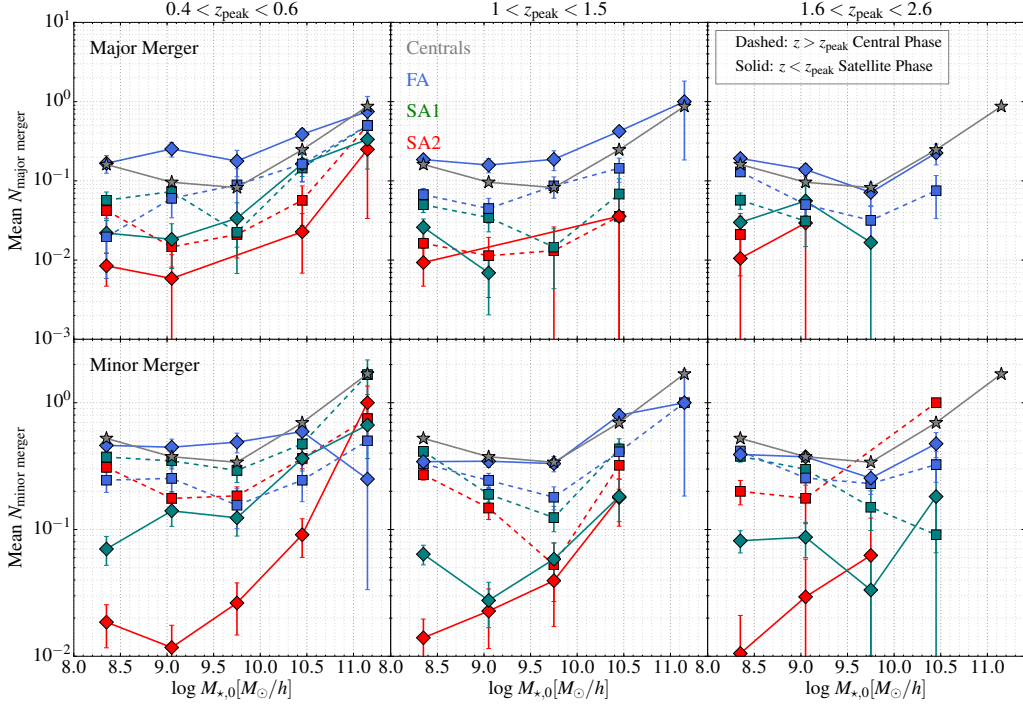


Figure 9. The mean number of major mergers and minor mergers experienced by the satellites in the three populations of halos (blue, green, and red) accreted at varying z_{peak} (from left to right columns) in TNG100. Major mergers are defined as $M_{\star, \text{prog}}/M_{\star, 0} > 0.2$; Minor merger are defined as $0.05 < M_{\star, \text{prog}}/M_{\star, 0} < 0.2$, where $M_{\star, 0}$ is the $z = 0$ stellar mass of a satellite in consideration, while $M_{\star, \text{prog}}$ is the maximum mass of its merging companion. Squares show the results for mergers occurring before z_{peak} , and diamonds are for mergers experienced after z_{peak} . The mean merger number of centrals at $z = 0$ are plotted as gray stars.

the stellar masses of the merging companion and the final galaxy at $z = 0$.

In Figure 9, we show the mean number of major and minor mergers as a function of $M_{\star, 0}$ for the three populations separately. In order to know when mergers usually happen, we show the results for mergers happening before and after z_{peak} separately. In general, the FA population experiences more major and minor mergers than the two SA populations of the same $M_{\star, 0}$ and z_{peak} in both central and satellite phases. For the FA population, both major and minor mergers occur more frequently in the satellite phase ($z < z_{\text{peak}}$) than in the central phase ($z > z_{\text{peak}}$). Furthermore, this trend holds in very wide $M_{\star, 0}$ and z_{peak} ranges as shown in the figure, while for the two SA populations, the trends are reversed. In addition, it also shows that the difference between the three populations in the central phase is much less than that in the satellite phase, consistent with the results for $f_{\text{ex situ}}$ (see Figure 8).

It is particularly interesting to inspect the results in the satellite phase in more detail. Major mergers for SA

satellites with $\log M_{\star, 0} < 10.0$ seem rather rare, with mean number of about 0.02, while for the FA satellites, the mean number of major mergers is about 10 times higher. Minor mergers occur much more frequently. The mean minor merger number for FA satellites with $\log M_{\star, 0} < 10.0$ is about 0.5, 10 times higher than that for SA satellites. For comparison, we also show the results for central galaxies at $z = 0$. These results suggest that, even in the satellite phase, galaxy mergers occur. In particular for FA satellites, the number of mergers that happen during the satellite phase can be higher/comparable to the total mergers happening for centrals. Note that for central galaxies, we count the merger events in their whole life. It is found that the mean number of major merger for centrals is usually lower than that for FA satellites (even if we count only the mergers in the satellite phase) and higher than that for the SA population. Furthermore, for minor mergers, the mean merger number for centrals is comparable to that for FA satellites and still higher than SA satellites.

4. IMPLICATIONS FOR SATELLITE EVOLUTION

Although hydrodynamical simulations cannot model all the details of the physical processes in galaxy formation, especially those occurring on small spatial scales within the interstellar medium, they still provide valuable information about how galaxies form and evolve, which may be useful for improving other galaxy formation models, such as SHAMs and semi-analytic models (Section 4.1 and 4.2). In fact, in simulations like TNG100 all the physical mechanisms that are important for the evolution of satellite and central galaxies are emerging phenomena and are not put in by hand: e.g. the hierarchical growth of structure, tidal and ram-pressure stripping, dynamical friction, etc. Moreover, when analyzing the efficiency of the quenching processes using observational data, we usually adopt some assumptions. Hydrodynamical simulations can also be used to check these assumptions (Section 4.3).

4.1. Implications for SHAM

In the simplest implementation of SHAMs (Kravtsov et al. 2004; Vale & Ostriker 2004; Conroy, Wechsler & Kravtsov 2006), galaxies and halos (subhalos) are rank ordered by $M_{*,0}$ and M_{halo} , and matched one by one according to their ranks so that $n_{\text{gal}}(> M_{*,0}) = n_{\text{halo}}(> M_{\text{h}})$ is satisfied. Here M_{halo} is usually taken as M_{peak} for satellites and M_0 for centrals. Instead of direct rank ordering, other SHAM implementations (Yang et al. 2012; Moster, Naab & White 2013; Behroozi, Wechsler & Conroy 2013) parameterize the SMHM relation for centrals at various redshifts. The parameters in the SMHM relation are constrained using the observed stellar mass function at various redshifts. However, these SHAM methods include several assumptions (see also Campbell et al. 2018 for a relevant discussion): (i) the rank ordered SHAM (rSHAM) assumes the same $z = 0$ SMHM relation for satellites and centrals, and that the SMHM relation is independent of the accretion time of satellites, (ii) the parameterized SHAM (pSHAM) assumes that satellites share the same z_{peak} SMHM relation as centrals, and there is neither gain nor loss of their stellar mass after accretion time, (iii) for both the rank-ordered and parameterized SHAM, at a given halo mass, the stellar mass of galaxies is independent of halo formation history.

More recently, Campbell et al. (2018) investigated the above halo-mass based SHAM models and found that they generally fail to reproduce the small-scale galaxy clustering signal. The authors tried to relax some of the assumptions in order to save those models, for example, by including orphan satellites, including satellite growth after accretion in pSHAM, and considering the dependence of the SMHM relation on halo formation history.

However, none of the above solutions alone can solve the “small-scale” clustering crisis, indicating a more detailed investigation of these assumptions is needed. Our results can provide a check for these (at least part of) assumptions made in those SHAM methods and help to provide insights for future improvements that can be done from the point of view of the TNG models.

Our studies (see Figure 2) support the assumptions made in rSHAM that satellites and centrals follow the same $z = 0$ SMHM relation when expressed as a function of M_{peak} for the satellites, and the relation for satellites is independent of accretion time. Our results further suggest that the scatter in the relation is also the same for centrals and satellites, and that the assumption that centrals and satellites share the same z_{peak} SMHM relation (where M_{peak} is adopted as the halo mass for satellites), which is usually adopted in pSHAM. These models usually ignore the mass growth of satellites in the satellite phase, which is apparently in conflict with our results and those by Engler et al. (in preparation, based on TNG50, TNG100, and TNG300). However, as shown in Figure 2, the mass growth after accretion does not change the SMHM relation too much when the latter is expressed for the satellites as a function of M_{peak} . This suggests that considering mass growth after accretion would not improve the model significantly. Moreover, these pSHAM models usually predict that the $M_{*,0} - M_{\text{peak}}$ relation for satellites is dependent on accretion time (Campbell et al. 2018), since in these models, the SMHM relation is usually dependent on redshift. In contrast, we find only weak or no dependence on z_{peak} in the TNG simulations.

We clearly show that the dependence of the SMHM relation on halo formation time is strong and significant, which is ignored by most SHAM models. In fact, Matthee et al. (2017) and Artale et al. (2018) have already found that the SMHM relation for central galaxies relies on the halo formation time. Our results (Figure 2) demonstrate a clear difference in the SMHM relation for satellites with different halo assembly histories (characterized by a_{nf}) at both $z = 0$ and z_{peak} . Since satellites with lower a_{nf} (younger) are usually accreted earlier than satellites with higher a_{nf} (higher), they are expected to reside in the inner regions of host halos at $z = 0$. This means that if we use the average SMHM relation to assign satellite mass, it might cause a systematic bias in the “small-scale” clustering. In addition, caution should be made when one assigns stellar mass to satellites taking into account halo formation history. A satellite with low a_{nf} and yet accreted at high z_{peak} may have the same z_{f} as an old satellite at low z_{peak} . Although they have the same z_{f} , they have very different

SMHM relations (see Figure 2). It thus would be better to adopt a_{nf} rather than z_{f} , since the former takes into account z_{peak} . A quantitative evaluation of how large the effects could be is certainly required.

4.2. Galaxy mergers for satellites

Galaxy mergers play an important role in galaxy formation and evolution. Major mergers can significantly change the galaxy morphology and may be responsible for the formation of massive ellipticals or bulges (see e.g. Torrey et al. 2014; Naab & Burkert 2003; Cox et al. 2006). Moreover, major mergers can trigger starbursts and accelerate the consumption of the cold gas reservoir (e.g. Mihos & Hernquist 1996; Barnes & Hernquist 1996; Cox et al. 2008). Minor mergers are also important, since they can increase sizes of passive galaxies (Shen et al. 2003; Oser et al. 2010; Shankar et al. 2013). The galaxy merger scenario is even thought to be able to reproduce the fundamental plane relation (Robertson et al. 2006).

In this paper, we find that satellites can experience frequent merger events. This is the case, however, exclusively for the FA satellites. Even in the satellite phase, major (minor) merger rate for FA satellites is higher than (comparable to) that for centrals. It means that after z_{peak} , satellites, exclusively FA satellites, may have even higher (or at least comparable) probability to change their morphology or increase their size via mergers than central galaxies of the same stellar mass. Moreover, major mergers likely play a role in consuming the cold gas and quenching star formation in satellite galaxies. More recently, Wang et al. (2019) found that the SDSS satellite and central galaxies have similar morphologies as long as halo mass and stellar mass are controlled, while SAM L-galaxies predicted a very different morphology between the two populations. One of the reasons for this discrepancy is that, in SAMs, by construction, mergers between satellites are assumed to be rare compared to the central-satellite merger (see e.g. Guo et al. 2011). Hydrodynamical simulations may provide some clues to improve the treatment of galaxy mergers in SAMs.

As shown in Figure 8, the ex situ stellar mass in the satellite phase (exclusively for FA satellites) usually grows rapidly around z_{peak} . Most of the ex situ accreted stars can be attributed to merger activities. It is interesting to know why galaxy mergers are boosted at this particular moment. FA halos are merging with their host halos at z_{peak} . It is possible that the orbits of the satellites in these FA halos are disrupted by the violent mergers between halos, and then galaxy mergers are enhanced in a short time. However, there is no such

signal for the two SA populations, which seems inconsistent with this scenario. In contrast to FA satellites, mergers for SA satellites in the satellite phase are apparently suppressed compared to central phases (Figure 8 and 9). This means that halo mergers are not necessary to lead to an increase in galaxy mergers. It is likely that whether mergers are enhanced or not depends on the halo formation history or halo inner structure. We will discuss this in a subsequent paper.

4.3. Implications for satellite quenching

Observationally, attempts have been made to constrain the efficiency of environmental processes by comparing satellites with centrals (Wetzel et al. 2013). The underlying assumption is that satellites at the accretion time share the same properties as centrals. Our results clearly show that centrals and satellites are very similar in the SMHM relation at z_{peak} (Figure 2) and even mass growth history before z_{peak} (Figure 3). They also share similar median gas to stellar mass ratios and specific star formation rates (Figure 4) and have a similar evolution of sSFR (Figure 5). Finally, they seem to have quite similar merging histories before z_{peak} (Figure 8). The simulation thus validates the assumptions adopted in the relevant studies.

To understand more about satellite quenching, we show the quenched fractions of satellite galaxies (see Section 2.2 on how quenched galaxies are defined) as a function of look-back time to t_{peak} in Figure 10. As before, we show the results for two stellar mass bins and three z_{peak} bins as examples. We can see strong dependences of quenching time scale on stellar mass, accretion time and satellite halo assembly history. More massive satellites are quenched in a longer time scale than less massive satellites for $\log M_{\star,0} < 10.0$. This suggests that environmental processes are more efficient for less massive satellites, as is to be expected. Satellites accreted early are quenched more quickly than those accreted later. One possible reason is that the gas environment in host halos at high redshift is more dense than those at low redshift. Therefore, the environmental effects are stronger at high redshift. Consistent with Figure 6, the time scale for satellites of high a_{nf} (older) to be quenched is longer than that for satellites of low a_{nf} (younger). There are two possible reasons. First, at accretion time, satellites in lower a_{nf} subhalos are more gas rich than satellites in higher a_{nf} subhalos. In the satellite phase, satellites that are in lower a_{nf} subhalos seem capable of acquiring more cold gas through accretion and even mergers (see Section 3.6).

From the evolution of the quenched fraction, we can see that the quenching time scale for satellites is up

to a few billion years long. For satellites with $8.5 < \log M_{\star,0} < 9.0$, to quench half of them requires about 4 Gyrs for $z_{\text{peak}} \sim 2$ and about 6.5 Gyrs for $z_{\text{peak}} \sim 1.2$. For satellites with $9.5 < \log M_{\star,0} < 10.0$, the corresponding time scales increase to 5 Gyrs and 8 Gyrs, respectively. More than 80% of satellites with $z_{\text{peak}} \sim 0.5$ are still active in forming stars today. In particular, we find that, after 2 Gyrs since accretion (i.e. the time of peak mass), only a small fraction of satellites is quenched. This suggests that these satellites can retain part of their hot gas and still acquire cold gas to fuel their star formation even when their dark halos stop growing. In practice, it can be expected that these time scales for quenching will be shorter and better captured, if the time of accretion was chosen to represent the time when a satellite crosses the virial radius instead of z_{peak} (see Donnari et al., in preparation).

5. SUMMARY

By using the cosmological hydrodynamical simulation TNG100, we studied in detail the formation histories of subhalos and the evolution of satellite galaxies lying therein. We use a scaled formation time, $a_{\text{nf}} \equiv (1 + z_f)/(1 + z_{\text{peak}})$, to characterize the formation history of a satellite subhalo before it is accreted by a massive host halo. Here z_f is the half mass formation time and z_{peak} is the accretion time. We choose satellites that have peak mass $M_{\text{peak}} > 10^{10} M_{\odot}/h$ and within host halos of $M_0 > 10^{11} M_{\odot}/h$. Our main results can be summarized as follows:

- (1) The scaled formation time distribution for subhalos in central phase is bimodal in TNG100. We divide them into three populations, fast accretion (FA, with $a_{\text{nf}} < 1.3$) and slow accretion (SA), which is sub-divided into SA1 with $1.3 < a_{\text{nf}} < 1.8$ and SA2 with $a_{\text{nf}} > 1.8$. At a given z_{peak} , subhalos with larger a_{nf} are older. Satellites accreted at high z_{peak} are dominated by the FA population, while satellites accreted at low z_{peak} are mainly SA halos. (Figure 1)
- (2) When expressed in terms of halo mass at z_{peak} for satellites, the median SMHM relation at $z = 0$ shows no significant difference between centrals and satellites; at accretion time, z_{peak} , the SMHM relation is also roughly the same between satellites and centrals. These are consistent with the assumptions made in SHAM methods. Besides, the SMHM relation shows very weak redshift evolution in TNG100. However, the SMHM relations are systematically different for young (lower a_{nf}) and

old (higher a_{nf}) subhalos, particularly at z_{peak} . (Figure 2)

- (3) The subhalo formation history has a significant impact on the stellar mass of satellite galaxies. At fixed halo mass at z_{peak} , the satellites in subhalos with lower a_{nf} (i.e. residing in younger subhalos) are more massive than those in the subhalos with higher a_{nf} (residing in older subhalos). After accretion, satellites continue to grow in stellar mass, with these in the subhalos with lower a_{nf} growing more comparing to those in the subhalos with higher a_{nf} . (see Figure 2 and 3)
- (4) The subhalo formation history also matters for the gas content and star-formation activities of satellites. At a given stellar mass at z_{peak} , satellites with lower a_{nf} subhalos (i.e. residing in younger subhalos) are more gas rich and have higher sSFRs than satellites in higher a_{nf} subhalos (Figure 4). After a short delay since accretion, satellite sSFRs decrease faster than for their central counterparts, indicating the role of host halo environments.
- (5) The quenching time scale depends on stellar mass, accretion time and subhalo formation history. It takes, e.g., on average up to 4 Gyr for half of those satellites having $z_{\text{peak}} \sim 2$ and about 6.5 Gyr for satellites having $z_{\text{peak}} \sim 1.2$ with $10^{8.5} < M_{\star,0} < 10^9 M_{\odot}/h$ at $z = 0$ to be quenched (Figure 10). Especially for satellites with lower a_{nf} subhalo, the quenching time is longer than satellites with higher a_{nf} subhalo. This is due to a combination of the higher gas mass in the central phase and the higher probability of mergers in the satellite phase for FA satellites.
- (6) The subhalo formation history has a dramatic impact on the satellite merger history. At a given z_{peak} , FA satellites experience merger events more frequently than SA satellites in both central and satellite phases. For FA satellites, mergers mainly happen in satellite phase, while for SA satellites, mergers mainly happen in the central phase (Figure 9). After being accreted by host halos, galaxy mergers for FA satellites are enhanced, while those for SA satellites are suppressed. For FA satellites, we find a burst of galaxy mergers and enhancement in star formation around z_{peak} , hinting that violent halo mergers might disrupt the orbits of galaxies in FA halos and trigger galaxy mergers. (Figure 7 and 8).

6. ACKNOWLEDGMENTS

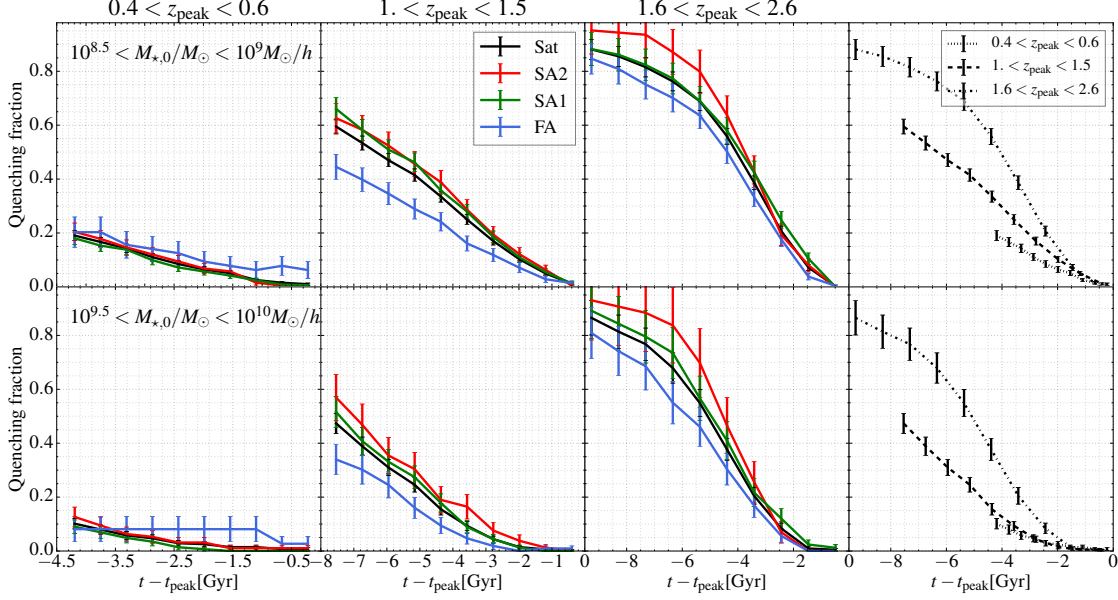


Figure 10. The quenched fractions of satellites as a function of the lookback time relative to the accretion time t_{peak} for satellites of different a_{nf} , z_{peak} and stellar mass in TNG100. The last column shows the quenching fractions for satellites accreted at three z_{peak} bins without distinguishing a_{nf} to highlight the dependence on z_{peak} .

J. Shi acknowledges the support of the Boya fellow provided by Peking University, helpful discussions with Lizhi Xie on the satellite-specific process and semi-analytic models. J. Shi also acknowledges discussions with Jeremy Tinker on satellite quenching. This work is supported by the National Key R&D Program of China (grant No. 2018YFA0404503), the National Natural Science Foundation of China (NSFC, Nos. 11733004, 11421303, 11890693, and 11522324),

the National Basic Research Program of China (973 Program)(2015CB857002), and the Fundamental Research Funds for the Central Universities. The work is supported by the Supercomputer Center of University of Science and Technology of China and the High-performance Computing Platform of Peking University in China. LCH was supported by the National Science Foundation of China (11721303, 11991052) and the National Key R&D Program of China (2016YFA0400702).

REFERENCES

- Artale M. C., Zehavi I., Contreras S., Norberg P., 2018, *MNRAS*, 480, 3978
- Ayromlou M., Nelson D., Yates R. M., Kauffmann G., White S. D. M., 2019, *MNRAS*, 487, 4313
- Bahé Y. M. et al., 2017, *MNRAS*, 470, 4186
- Bahé Y. M., McCarthy I. G., 2015, *MNRAS*, 447, 969
- Bahé Y. M. et al., 2019, *MNRAS*, 485, 2287
- Barnes J. E., Hernquist L., 1996, *ApJ*, 471, 115
- Barro G. et al., 2017, *ApJ*, 840, 47
- Behroozi P. S., Conroy C., Wechsler R. H., 2010, *ApJ*, 717, 379
- Behroozi P. S., Wechsler R. H., Conroy C., 2013, *ApJ*, 770, 57
- Berlind A. A., Weinberg D. H., 2002, *ApJ*, 575, 587
- Bower R. G., Benson A. J., Malbon R., Helly J. C., Frenk C. S., Baugh C. M., Cole S., Lacey C. G., 2006, *MNRAS*, 370, 645
- Bray A. D. et al., 2016, *MNRAS*, 455, 185
- Calderon V. F., Berlind A. A., Sinha M., 2018, *MNRAS*, 480, 2031
- Calette A. R., Avila-Reese V., Rodríguez-Puebla A., Hernández-Toledo H., Papastergis E., 2018, *RMxAA*, 54, 443
- Campbell D., van den Bosch F. C., Padmanabhan N., Mao Y.-Y., Zentner A. R., Lange J. U., Jiang F., Villarreal A., 2018, *MNRAS*, 477, 359
- Chandrasekhar S., 1943a, *ApJ*, 97, 255
- , 1943b, *ApJ*, 97, 263
- , 1943c, *ApJ*, 98, 54

- Conroy C., Wechsler R. H., Kravtsov A. V., 2006, *ApJ*, 647, 201
- Cox T. J., Dutta S. N., Di Matteo T., Hernquist L., Hopkins P. F., Robertson B., Springel V., 2006, *ApJ*, 650, 791
- Cox T. J., Jonsson P., Somerville R. S., Primack J. R., Dekel A., 2008, *MNRAS*, 384, 386
- Croton D. J. et al., 2006, *MNRAS*, 365, 11
- Davis M., Efstathiou G., Frenk C. S., White S. D. M., 1985, *ApJ*, 292, 371
- De Lucia G., Blaizot J., 2007, *MNRAS*, 375, 2
- Donnari M. et al., 2019, *MNRAS*, 485, 4817
- Fall S. M., Efstathiou G., 1980, *MNRAS*, 193, 189
- Farouki R., Shapiro S. L., 1981, *ApJ*, 243, 32
- Font A. S. et al., 2008, *MNRAS*, 389, 1619
- Genel S. et al., 2014, *MNRAS*, 445, 175
- Genzel R. et al., 2017, *Nature*, 543, 397
- , 2015, *ApJ*, 800, 20
- Gnedin O. Y., Hernquist L., Ostriker J. P., 1999, *ApJ*, 514, 109
- Gunn J. E., Gott, J. Richard I., 1972, *ApJ*, 176, 1
- Guo Q. et al., 2011, *MNRAS*, 413, 101
- Guo Q., White S., Li C., Boylan-Kolchin M., 2010, *MNRAS*, 404, 1111
- Henriques B. M. B., White S. D. M., Thomas P. A., Angulo R., Guo Q., Lemson G., Springel V., Overzier R., 2015, *MNRAS*, 451, 2663
- Henriques B. M. B., White S. D. M., Thomas P. A., Angulo R. E., Guo Q., Lemson G., Wang W., 2017, *MNRAS*, 469, 2626
- Hirschmann M., De Lucia G., Wilman D., Weinmann S., Iovino A., Cucciati O., Zibetti S., Villalobos Á., 2014, *MNRAS*, 444, 2938
- Jing Y. P., Mo H. J., Börner G., 1998, *ApJ*, 494, 1
- Jung S. L., Choi H., Wong O. I., Kimm T., Chung A., Yi S. K., 2018, *ApJ*, 865, 156
- Kang X., van den Bosch F. C., 2008, *ApJL*, 676, L101
- Kauffmann G., Li C., Zhang W., Weinmann S., 2013, *MNRAS*, 430, 1447
- Kravtsov A. V., Berlind A. A., Wechsler R. H., Klypin A. A., Gottlöber S., Allgood B. o., Primack J. R., 2004, *ApJ*, 609, 35
- Lu Z., Mo H. J., Lu Y., Katz N., Weinberg M. D., van den Bosch F. C., Yang X., 2015, *MNRAS*, 450, 1604
- Makino J., Hut P., 1997, *ApJ*, 481, 83
- Mandelbaum R., Seljak U., Kauffmann G., Hirata C. M., Brinkmann J., 2006, *MNRAS*, 368, 715
- Marinacci F., Vogelsberger M., Kannan R., Mocz P., Pakmor R., Springel V., 2018, *MNRAS*, 476, 2476
- Matthee J., Schaye J., Crain R. A., Schaller M., Bower R., Theuns T., 2017, *MNRAS*, 465, 2381
- Mihos J. C., Harding P., Feldmeier J., Morrison H., 2005, *ApJL*, 631, L41
- Mihos J. C., Hernquist L., 1996, *ApJ*, 464, 641
- More S., van den Bosch F. C., Cacciato M., Skibba R., Mo H. J., Yang X., 2011, *MNRAS*, 410, 210
- Moster B. P., Naab T., White S. D. M., 2013, *MNRAS*, 428, 3121
- Naab T., Burkert A., 2003, *ApJ*, 597, 893
- Naiman J. P. et al., 2018, *MNRAS*, 477, 1206
- Nelson D. et al., 2019a, *MNRAS*, 490, 3234
- , 2018, *MNRAS*, 475, 624
- , 2019b, *Computational Astrophysics and Cosmology*, 6, 2
- Newman A. B., Ellis R. S., Bundy K., Treu T., 2012, *ApJ*, 746, 162
- Oser L., Ostriker J. P., Naab T., Johansson P. H., Burkert A., 2010, *ApJ*, 725, 2312
- Ostriker J. P., Tremaine S. D., 1975, *ApJL*, 202, L113
- Pannella M. et al., 2009, *ApJ*, 701, 787
- Pasquali A., Smith R., Gallazzi A., De Lucia G., Zibetti S., Hirschmann M., Yi S. K., 2019, *MNRAS*, 484, 1702
- Peng Y., Maiolino R., Cochrane R., 2015, *Nature*, 521, 192
- Peng Y.-j. et al., 2010, *ApJ*, 721, 193
- Peng Y.-j., Lilly S. J., Renzini A., Carollo M., 2012, *ApJ*, 757, 4
- Pillepich A. et al., 2018a, *MNRAS*, 475, 648
- , 2019, *MNRAS*, 490, 3196
- , 2018b, *MNRAS*, 473, 4077
- Planck Collaboration et al., 2016, *A&A*, 594, A13
- Price S. H. et al., 2019, *arXiv e-prints*, arXiv:1902.09554
- Rees M. J., Ostriker J. P., 1977, *MNRAS*, 179, 541
- Rhee J., Smith R., Choi H., Yi S. K., Jaffé Y., Candlish G., Sánchez-Jánssen R., 2017, *ApJ*, 843, 128
- Robertson B., Cox T. J., Hernquist L., Franx M., Hopkins P. F., Martini P., Springel V., 2006, *ApJ*, 641, 21
- Rodríguez-Gomez V. et al., 2015, *MNRAS*, 449, 49
- , 2017, *MNRAS*, 467, 3083
- Rodríguez-Puebla A., Primack J. R., Avila-Reese V., Faber S. M., 2017, *MNRAS*, 470, 651
- Sales L. V. et al., 2015, *MNRAS*, 447, L6
- Shankar F., Marulli F., Bernardi M., Mei S., Meert A., Vikram V., 2013, *MNRAS*, 428, 109
- Shen S., Mo H. J., White S. D. M., Blanton M. R., Kauffmann G., Voges W., Brinkmann J., Csabai I., 2003, *MNRAS*, 343, 978
- Shi J., Wang H., Mo H. J., Xie L., Wang X., Lapi A., Sheth R. K., 2018, *ApJ*, 857, 127
- Simha V., Weinberg D. H., Davé R., Gnedin O. Y., Katz N., Kereš D., 2009, *MNRAS*, 399, 650

- Springel V., 2010, *ARA&A*, 48, 391
- Springel V. et al., 2018, *MNRAS*, 475, 676
- Springel V., White S. D. M., Tormen G., Kauffmann G., 2001, *MNRAS*, 328, 726
- Stark D. P., Schenker M. A., Ellis R., Robertson B., McLure R., Dunlop J., 2013, *ApJ*, 763, 129
- Tacchella S. et al., 2019, *MNRAS*, 487, 5416
- Tacconi L. J. et al., 2018, *ApJ*, 853, 179
- Tadaki K. et al., 2017, *ApJ*, 834, 135
- Terrazas B. A. et al., 2019, arXiv e-prints, arXiv:1906.02747
- Tinker J. L., Hahn C., Mao Y.-Y., Wetzel A. R., Conroy C., 2018, *MNRAS*, 477, 935
- Tinker J. L., Norberg P., Weinberg D. H., Warren M. S., 2007, *ApJ*, 659, 877
- Torrey P., Vogelsberger M., Genel S., Sijacki D., Springel V., Hernquist L., 2014, *MNRAS*, 438, 1985
- Vale A., Ostriker J. P., 2004, *MNRAS*, 353, 189
- van de Voort F., Schaye J., Booth C. M., Dalla Vecchia C., 2011, *MNRAS*, 415, 2782
- van den Bosch F. C., Aquino D., Yang X., Mo H. J., Pasquali A., McIntosh D. H., Weinmann S. M., Kang X., 2008, *MNRAS*, 387, 79
- Vogelsberger M., Genel S., Sijacki D., Torrey P., Springel V., Hernquist L., 2013, *MNRAS*, 436, 3031
- Vogelsberger M. et al., 2014a, *Nature*, 509, 177
- , 2014b, *MNRAS*, 444, 1518
- Vogelsberger M., Marinacci F., Torrey P., Puchwein E., 2019, arXiv e-prints, arXiv:1909.07976
- Wang E. et al., 2018a, *ApJ*, 860, 102
- Wang E., Wang H., Mo H., van den Bosch F. C., Lim S. H., Wang L., Yang X., Chen S., 2018b, *ApJ*, 864, 51
- Wang E., Wang H., Mo H., van den Bosch F. C., Yang X., 2019, arXiv e-prints, arXiv:1912.05969
- Wang H. et al., 2018c, *ApJ*, 852, 31
- Wang L., Jing Y. P., 2010, *MNRAS*, 402, 1796
- Wang Y., Yang X., Mo H. J., van den Bosch F. C., 2007, *ApJ*, 664, 608
- Wechsler R. H., Tinker J. L., 2018, *ARA&A*, 56, 435
- Weinberger R., Springel V., Pakmor R., 2019, arXiv e-prints, arXiv:1909.04667
- Weinberger R. et al., 2018, *MNRAS*, 479, 4056
- Weinmann S. M., Kauffmann G., van den Bosch F. C., Pasquali A., McIntosh D. H., Mo H., Yang X., Guo Y., 2009, *MNRAS*, 394, 1213
- Weinmann S. M., Kauffmann G., von der Linden A., De Lucia G., 2010, *MNRAS*, 406, 2249
- Weinmann S. M., van den Bosch F. C., Yang X., Mo H. J., 2006, *MNRAS*, 366, 2
- Wetzel A. R., Cohn J. D., White M., 2009, *MNRAS*, 395, 1376
- Wetzel A. R., Tinker J. L., Conroy C., van den Bosch F. C., 2013, *MNRAS*, 432, 336
- Wetzel A. R., White M., 2010, *MNRAS*, 403, 1072
- White S. D. M., Rees M. J., 1978, *MNRAS*, 183, 341
- Wright R. J., Lagos C. d. P., Davies L. J. M., Power C., Trayford J. W., Wong O. I., 2019, *MNRAS*, 487, 3740
- Yang X., Mo H. J., van den Bosch F. C., 2003, *MNRAS*, 339, 1057
- , 2008, *ApJ*, 676, 248
- , 2009, *ApJ*, 693, 830
- Yang X., Mo H. J., van den Bosch F. C., Jing Y. P., 2005, *MNRAS*, 356, 1293
- Yang X., Mo H. J., van den Bosch F. C., Zhang Y., Han J., 2012, *ApJ*, 752, 41
- Yun K. et al., 2019, *MNRAS*, 483, 1042
- Zehavi I., Contreras S., Padilla N., Smith N. J., Baugh C. M., Norberg P., 2018, *ApJ*, 853, 84
- Zhao D. H., Jing Y. P., Mo H. J., Börner G., 2003, *ApJL*, 597, L9
- Zheng Z., Coil A. L., Zehavi I., 2007, *ApJ*, 667, 760
- Zu Y., Mandelbaum R., 2015, *MNRAS*, 454, 1161